Supporting Information for

Anthracene-9-carboxylic acid-based [Cu_{20}] cluster templated by bromine anion for heterogeneous catalytic chemical fixation of carbon dioxide

Dapeng Dong, [a] Xueqin Tian, [b] Pengyan Wu, [b] Jian Wang, [b]* Jindou Huang,[a] Haiyan Zhao, [a] Dedi Liu [a] and Zhenyi Zhang [a]*

[a] Key Laboratory of New Energy and Rare Earth Resource Utilization of State Ethnic Affairs Commission, Key Laboratory of Photosensitive Materials and Devices of Liaoning Province, School of Physics and Materials Engineering, Dalian Nationalities University, 18 Liaohe West Road, Dalian 116600, China

[b] School of Chemistry and Materials Science, Jiangsu Key Laboratory of Green Synthetic Chemistry for Functional Materials, Jiangsu Normal University, Xuzhou, 221116, China

Experimental Section

Materials and Characterizations

All the chemicals were purchased from commercial sources and used without any further purification. The elemental analyses of C, H and N were performed on a Vario EL III elemental analyzer. ^{1}H NMR spectra were measured on a Bruker-400 spectrometer with Me_4Si as an internal standard. X-Ray powder diffraction (XRD) patterns of the [Cu_{20}] was recorded on a Rigaku D/max-2400 X−ray powder diffractometer (Japan) using Cu-Kα (λ = 1.5405 Å) radiation. FT−IR spectra were recorded as KBr pellets on JASCO FT/IR−430. Thermogravimetric analysis (TGA) was carried out at a ramp rate of 5 °C/min in static air flow with a Rigaku Thermo plus TG-8120 instrument. The morphologies of the prepared samples were recorded by a Field Emission Scanning Electron Microscopy (SEM) of Hitachi SU8010. Samples were treated via Pt sputtering for 90 s before observation. Transmission electron microscopy (TEM; JEOL JEM-2100) were used to acquire the morphology of the catalyst. The contents of metal ions were measured by inductively coupled plasma mass spectrometry (ICP-MS; Leeman PROFILE SPEC).

Pyridine FT-IR determination method

The powder sample of 10 mg was pressed into thin slices and fixed in an infrared pool. After vacuum purification (110 °C, 1 × 10^{-3} Pa) for 2 hours, the samples were cooled to room temperature, and the scanning spectra were used as background. After pyridine was adsorbed at room temperature, the temperature was raised to the 150 ° C for vacuum desorption (1 × 10^{-3} Pa) for half an hour, and then cooled to room temperature, respectively, the infrared spectra of 1700 ~ 1400 cm^{-1} wave number region were recorded. The Lewis acid was characterized by 1447 cm^{-1} peak.

Crystallographic studies

Data collections for [Cu_{20}] and [Cu_2] were performed on a Bruker AXS Smart APEX II CCD X–diffractometer equipped with graphite monochromated Mo–Kα radiation (λ = 0.71073Å) at 293 ± 2 K. An empirical absorption correction was applied using the SADABS program. The structures were solved by direct methods and refined by full matrix least–squares on F^2 by using the program SHELXL–2014. All non-hydrogen atoms were refined with anisotropic thermal parameters. Hydrogen atoms of organic ligands were generated geometrically with fixed isotropic thermal parameters, and included in the structure factor calculations. Details of crystallographic data and structural refinements of [Cu_{20}] and [Cu_2] were summarized in Table S1. Selected bond lengths (Å) and bond angles (º) of [Cu_{20}] and [Cu_2] were listed in Table S2. CCDC 2180593 and 2180594 containing the supplementary crystallographic data for this paper. These data can be obtained free of charge www.ccdc.cam.ac.uk/conts/retrieving.html.

Computational method

In the present work, all electronic structure calculations were carried out with the Gaussian 09 program suite. Geometry optimizations of the studied Cu complex were implemented using DFT method. The Becke's three-parameter hybrid exchange functional with Lee-Yang-Parr gradient-corrected correlation (B3LYP functional) and 6-31g* is selected for the structure optimization and energy calculations. The self-consistent field (SCF) convergence thresholds of the energy for geometry optimization were used the default setting (10^{-6}).

Table S1. Crystallographic data for [Cu_{20}] and [Cu_2].

Compound	[Cu_{20}]	[Cu_2]
formula	$C_{213}H_{239}Br_7Cu_{20}N_{14}O_{56}$	$C_{90}H_{56}Cu_2O_{12}$
Fw	5721.34	1456.42
crystal system	Monoclinic	Monoclinic
Space group	$P2_1/n$	$P2_1/c$
a, Å	21.0945(4)	11.2467(12)
b, Å	25.7195(5)	13.1263(15)
c, Å	22.2256(5)	23.491(3)
α, °	90	90
β, °	95.7709(13)	98.018(2)
γ, °	90	90
V, Å^3	11997.2(4)	3434.0(7)
Z	2	2
D_c, g/cm^3	1.584	1.409
μ (Mo K_α), mm^{-1}	2.972	0.688
θ_{min}, θ_{max} , °	1.584, 27.531	1.751, 27.557
no. total reflns.	146627	24591
no. uniq. reflns (R_{int})	27455 (0.1561)	7893 (0.0641)
no. obs. [I≥2σ(I)]	13013	4582
no. params	1386	469
$R1$,$wR2$ [I≥2σ(I)]	0.0722, 0.1838	0.0488, 0.1005
$R1$,$wR2$ (all data)	0.1770, 0.2306	0.1033, 0.1235
GOF	1.049	0.986

Table S2 Selected bond lengths (Å) and angles (º) for [Cu_{20}] and [Cu_2].

[Cu_{20}]			
Cu(1)-O(18)	1.915(6)	Cu(1)-O(17)	1.960(5)
Cu(1)-O(19)	1.976(5)	Cu(1)-O(14)	1.998(5)
Cu(1)-O(12)	2.231(6)	Cu(2)-O(1)	1.969(6)
Cu(2)-O(4)	1.982(6)	Cu(2)-O(17)	2.031(5)
Cu(2)-O(19)	2.045(5)	Cu(2)-O(11)	2.279(6)
Cu(2)-O(20)	2.326(6)	Cu(3)-O(22)	1.936(6)
Cu(3)-O(20)	1.941(6)	Cu(3)-O(23)	1.986(5)
Cu(3)-O(19)	1.986(5)	Cu(3)-O(2)	2.330(6)
Cu(4)-O(20)	1.916(5)	Cu(4)-O(16)	1.922(5)
Cu(4)-O(17)	2.006(5)	Cu(4)-O(24)#1	2.009(5)
Cu(4)-O(3)	2.273(6)	Cu(5)-O(5)	1.934(6)
Cu(5)-N(1)	1.985(8)	Cu(5)-O(24)#1	2.024(5)
Cu(5)-O(25)#1	2.046(6)	Cu(5)-O(16)	2.231(5)
Cu(6)-O(22)#1	1.941(5)	Cu(6)-O(16)	1.955(5)
Cu(6)-O(15)	1.976(5)	Cu(6)-O(25)#1	1.987(5)
Cu(6)-O(6)	2.284(6)	Cu(7)-O(8)	1.970(6)
Cu(7)-N(2)	2.005(7)	Cu(7)-O(21)	2.006(6)
Cu(7)-O(14)	2.098(5)	Cu(7)-O(9)	2.248(7)
Cu(8)-O(18)	1.915(6)	Cu(8)-O(25)	1.972(5)
Cu(8)-O(24)	1.975(5)	Cu(8)-O(21)	1.980(6)
Cu(8)-O(7)	2.236(6)	Cu(9)-O(14)	1.951(5)
Cu(9)-O(21)	1.953(6)	Cu(9)-O(23)#1	1.970(6)
Cu(9)-O(15)	1.978(5)	Cu(9)-O(10)	2.384(7)
Cu(10)-N(3)	1.965(8)	Cu(10)-O(13)	1.968(7)
Cu(10)-O(15)	1.995(5)	Cu(10)-O(23)#1	2.031(6)
O(18)-Cu(1)-O(17)	175.7(2)	O(18)-Cu(1)-O(19)	96.0(2)
O(17)-Cu(1)-O(19)	81.7(2)	O(18)-Cu(1)-O(14)	86.3(2)
O(17)-Cu(1)-O(14)	95.9(2)	O(19)-Cu(1)-O(14)	176.9(2)
O(18)-Cu(1)-O(12)	91.9(2)	O(17)-Cu(1)-O(12)	91.8(2)
O(19)-Cu(1)-O(12)	93.4(2)	O(14)-Cu(1)-O(12)	88.5(2)

O(1)-Cu(2)-O(4)	88.7(2)	O(1)-Cu(2)-O(17)	173.2(2)
O(4)-Cu(2)-O(17)	95.5(2)	O(1)-Cu(2)-O(19)	97.2(2)
O(4)-Cu(2)-O(19)	173.3(2)	O(17)-Cu(2)-O(19)	78.3(2)
O(1)-Cu(2)-O(11)	85.8(2)	O(4)-Cu(2)-O(11)	89.8(2)
O(17)-Cu(2)-O(11)	99.5(2)	O(19)-Cu(2)-O(11)	93.8(2)
O(1)-Cu(2)-O(20)	97.6(2)	O(4)-Cu(2)-O(20)	100.5(2)
O(17)-Cu(2)-O(20)	76.4(2)	O(19)-Cu(2)-O(20)	75.6(2)
O(11)-Cu(2)-O(20)	169.1(2)	O(22)-Cu(3)-O(20)	174.1(2)
O(22)-Cu(3)-O(23)	85.3(2)	O(20)-Cu(3)-O(23)	91.0(2)
O(22)-Cu(3)-O(19)	97.3(2)	O(20)-Cu(3)-O(19)	86.3(2)
O(23)-Cu(3)-O(19)	177.3(2)	O(22)-Cu(3)-O(2)	95.3(2)
O(20)-Cu(3)-O(2)	89.4(2)	O(23)-Cu(3)-O(2)	92.9(2)
O(19)-Cu(3)-O(2)	87.2(2)	O(20)-Cu(4)-O(16)	177.0(2)
O(20)-Cu(4)-O(17)	87.2(2)	O(16)-Cu(4)-O(17)	94.9(2)
O(20)-Cu(4)-O(24)#1	93.9(2)	O(16)-Cu(4)-O(24)#1	84.1(2)
O(17)-Cu(4)-O(24)#1	177.7(2)	O(20)-Cu(4)-O(3)	91.8(2)
O(16)-Cu(4)-O(3)	90.5(2)	O(17)-Cu(4)-O(3)	88.0(2)
O(24)#1-Cu(4)-O(3)	90.0(2)	O(5)-Cu(5)-N(1)	92.3(3)
O(5)-Cu(5)-O(24)#1	174.0(2)	N(1)-Cu(5)-O(24)#1	91.6(3)
O(5)-Cu(5)-O(25)#1	99.0(3)	N(1)-Cu(5)-O(25)#1	159.4(3)
O(24)#1-Cu(5)-O(25)#1	78.8(2)	O(5)-Cu(5)-O(16)	97.8(2)
N(1)-Cu(5)-O(16)	118.1(3)	O(24)#1-Cu(5)-O(16)	76.3(2)
O(25)#1-Cu(5)-O(16)	77.5(2)	O(22)#1-Cu(6)-O(16)	174.3(2)
O(22)#1-Cu(6)-O(15)	86.2(2)	O(16)-Cu(6)-O(15)	91.8(2)
O(22)#1-Cu(6)-O(25)#1	96.0(2)	O(16)-Cu(6)-O(25)#1	85.7(2)
O(15)-Cu(6)-O(25)#1	176.1(2)	O(22)#1-Cu(6)-O(6)	98.5(2)
O(16)-Cu(6)-O(6)	86.8(2)	O(15)-Cu(6)-O(6)	92.0(2)
O(25)#1-Cu(6)-O(6)	91.0(2)	O(8)-Cu(7)-N(2)	94.0(3)
O(8)-Cu(7)-O(21)	95.1(2)	N(2)-Cu(7)-O(21)	169.6(3)
O(8)-Cu(7)-O(14)	164.9(2)	N(2)-Cu(7)-O(14)	93.0(3)
O(21)-Cu(7)-O(14)	77.0(2)	O(8)-Cu(7)-O(9)	94.2(3)
N(2)-Cu(7)-O(9)	92.8(3)	O(21)-Cu(7)-O(9)	91.5(2)
O(14)-Cu(7)-O(9)	98.8(2)	O(18)-Cu(8)-O(25)	96.5(2)

O(18)-Cu(8)-O(24)	176.4(2)	O(25)-Cu(8)-O(24)	81.7(2)
O(18)-Cu(8)-O(21)	87.4(2)	O(25)-Cu(8)-O(21)	174.8(2)
O(24)-Cu(8)-O(21)	94.3(2)	O(18)-Cu(8)-O(7)	93.1(2)
O(25)-Cu(8)-O(7)	94.0(2)	O(24)-Cu(8)-O(7)	90.0(2)
O(21)-Cu(8)-O(7)	89.3(2)	O(14)-Cu(9)-O(21)	81.8(2)
O(14)-Cu(9)-O(23)#1	176.9(2)	O(21)-Cu(9)-O(23)#1	97.8(2)
O(14)-Cu(9)-O(15)	98.6(2)	O(21)-Cu(9)-O(15)	179.4(2)
O(23)#1-Cu(9)-O(15)	81.9(2)	O(14)-Cu(9)-O(10)	96.1(2)
O(21)-Cu(9)-O(10)	99.4(2)	O(23)#1-Cu(9)-O(10)	80.9(2)
O(15)-Cu(9)-O(10)	81.1(2)	N(3)-Cu(10)-O(13)	90.5(3)
N(3)-Cu(10)-O(15)	168.5(3)	O(13)-Cu(10)-O(15)	98.7(3)
N(3)-Cu(10)-O(23)#1	92.2(3)	O(13)-Cu(10)-O(23)#1	169.9(3)
O(15)-Cu(10)-O(23)#1	80.0(2)		
[Cu_2]			
Cu(1)-O(4)	1.9460(18)	Cu(1)-O(3)#2	1.9514(19)
Cu(1)-O(2)#2	1.9731(19)	Cu(1)-O(1)	1.9991(19)
Cu(1)-O(5)	2.149(2)		
O(4)-Cu(1)-O(3)#2	169.79(9)	O(4)-Cu(1)-O(2)#2	89.75(8)
O(3)#2-Cu(1)-O(2)#2	92.20(8)	O(4)-Cu(1)-O(1)	89.59(8)
O(3)#2-Cu(1)-O(1)	86.76(8)	O(2)#2-Cu(1)-O(1)	170.10(8)
O(4)-Cu(1)-O(5)	96.51(8)	O(3)#2-Cu(1)-O(5)	93.02(8)
O(2)#2-Cu(1)-O(5)	100.04(8)	O(1)-Cu(1)-O(5)	89.85(8)

Symmetry transformations used to generate equivalent atoms:

#1 -x,-y+2,-z-3; #2 -x+1,-y,-z+1.

Figure S1. Structure unit of [Cu_2] showing the O─H…O hydrogen bond. Atomic scheme: Cu, turquiose; O, red; C, gray; H, light gray.

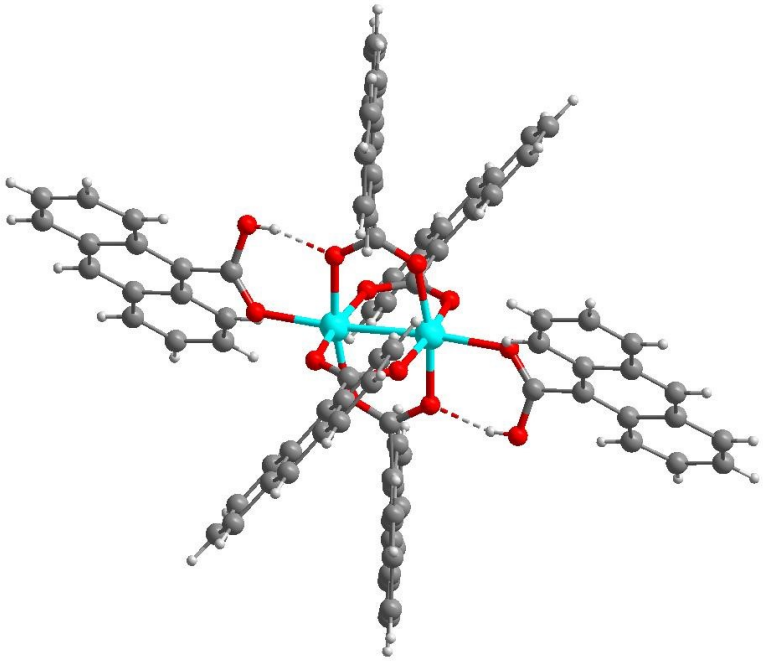

Figure S2. Packing diagram of [Cu_2] along the *b*-axis. Atomic scheme: Cu, blue; O, red; C, gray; H, light gray.

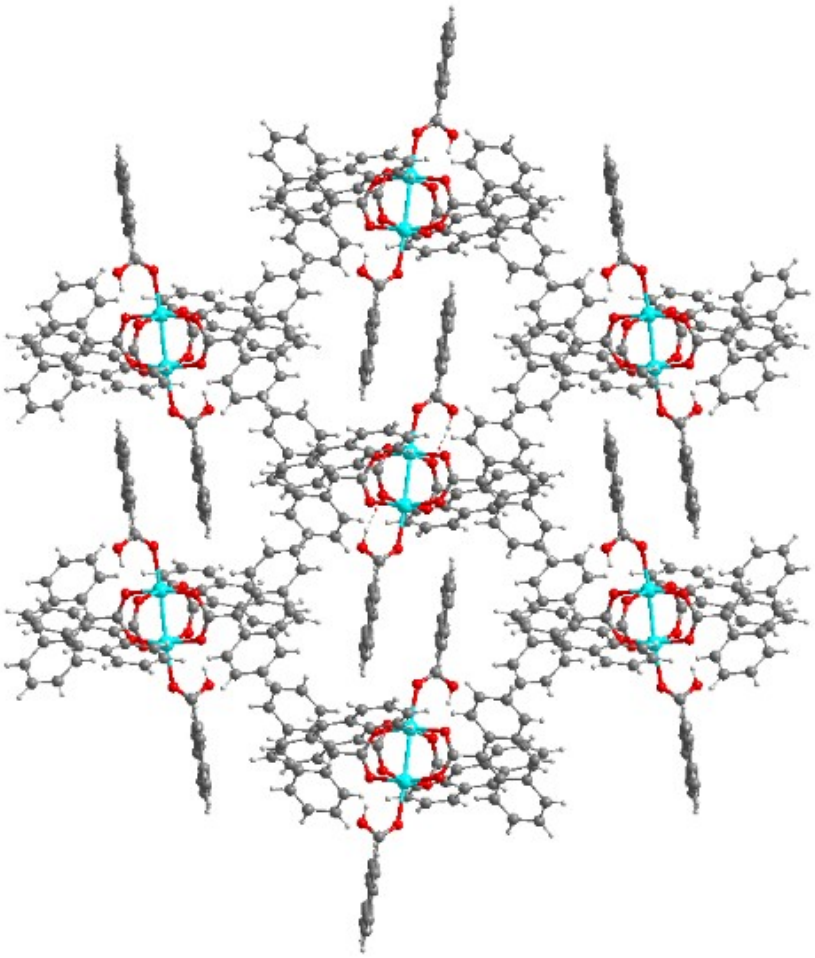

Figure S3. Powder XRD patterns of [Cu_{20}] simulated from single-crystal X-ray diffraction results, the as-synthesized [Cu_{20}], and [Cu_{20}] after catalysis.

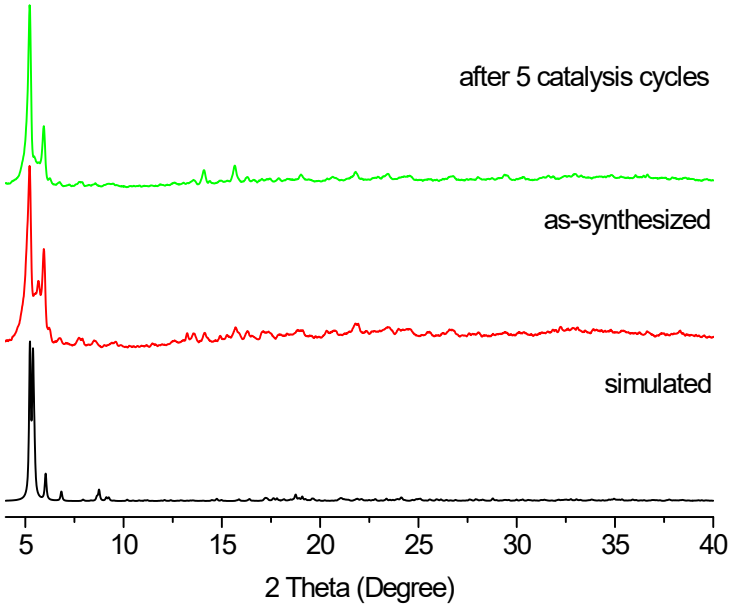

Figure S4. The TG curve of [Cu_{20}] ranging from room temperature to 800 °C.

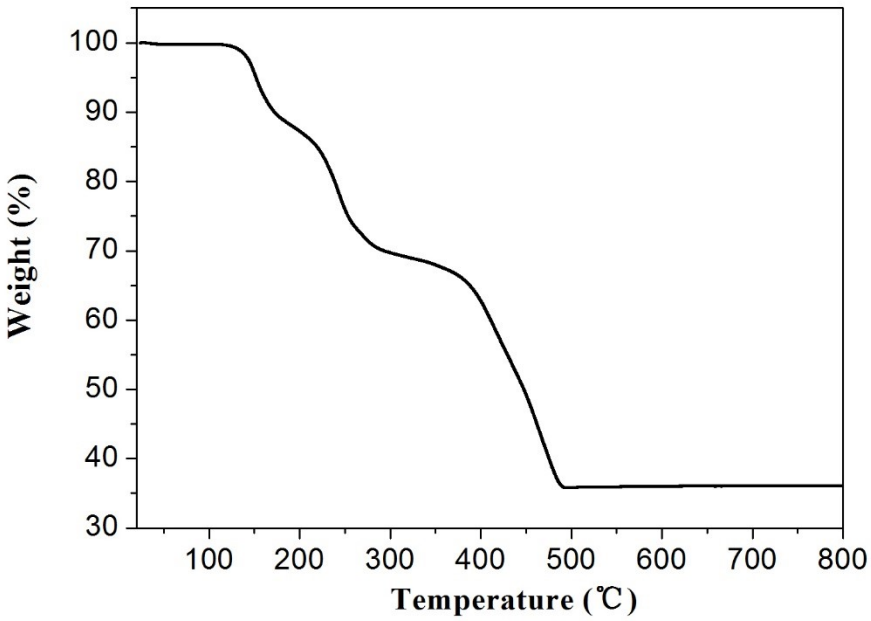

Figure S5. XPS spectra for [Cu_{20}] and [Cu_{20}] after treated with epichlorohydrin.

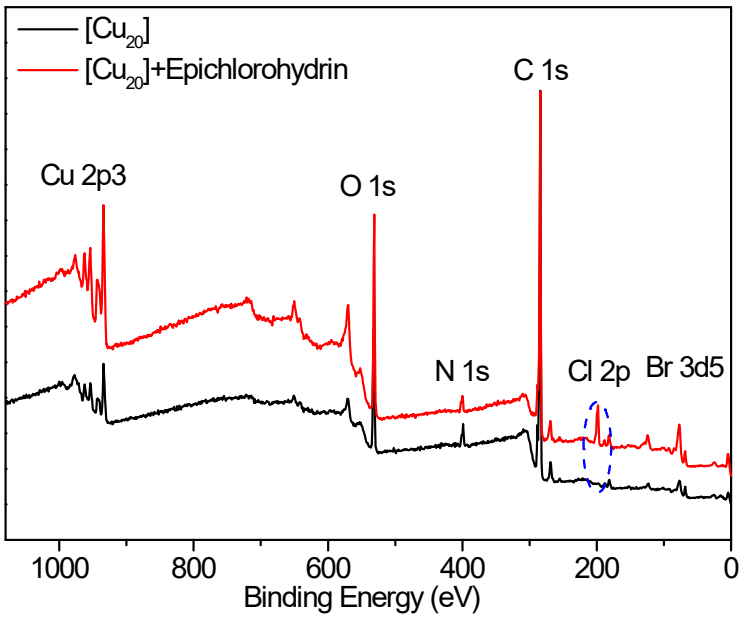

Figure S6. FT-IR spectra of [Cu_{20}] (black), [Cu_{20}] impregnated with epichlorohydrin (red) and epichlorohydrin (green).

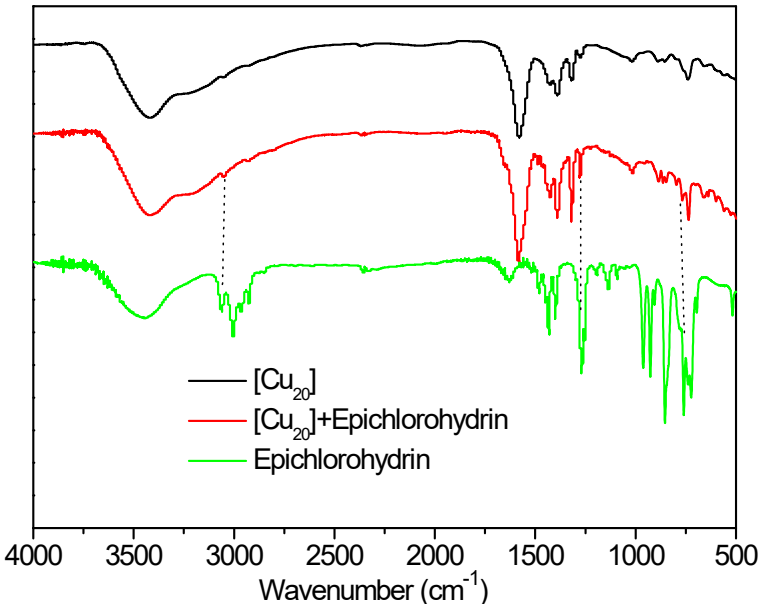

Figure S7. The TEM images of [Cu_{20}] (a) and [Cu_{20}] impregnated with epichlorohydrin (b).

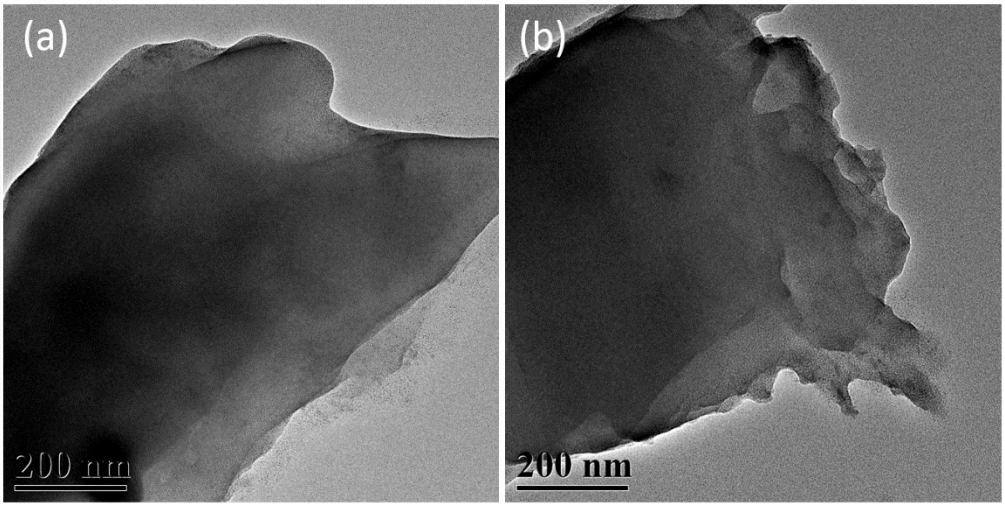

Figure S8. The PY-IR spectra of [Cu_{20}] and [Cu_2].

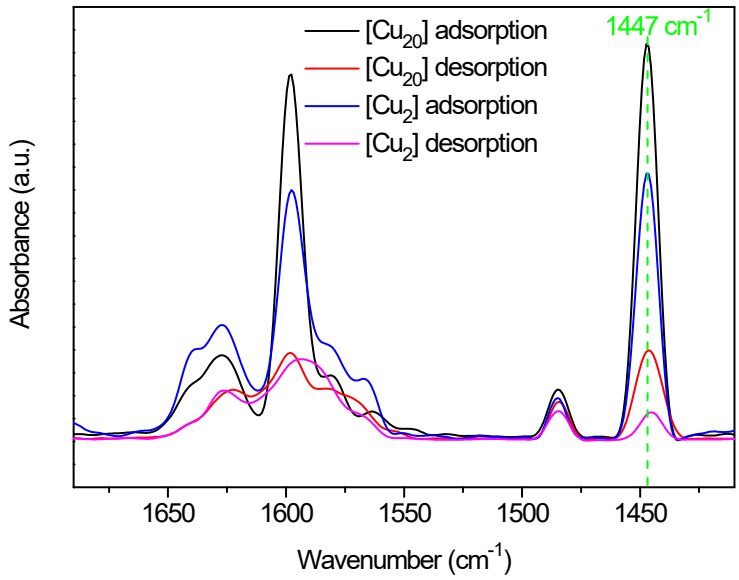

Figure S9. Yields of 4-(chloromethyl)-1,3-dioxolan-2-one catalyzed by the filtered solution after 1 h of the reaction.

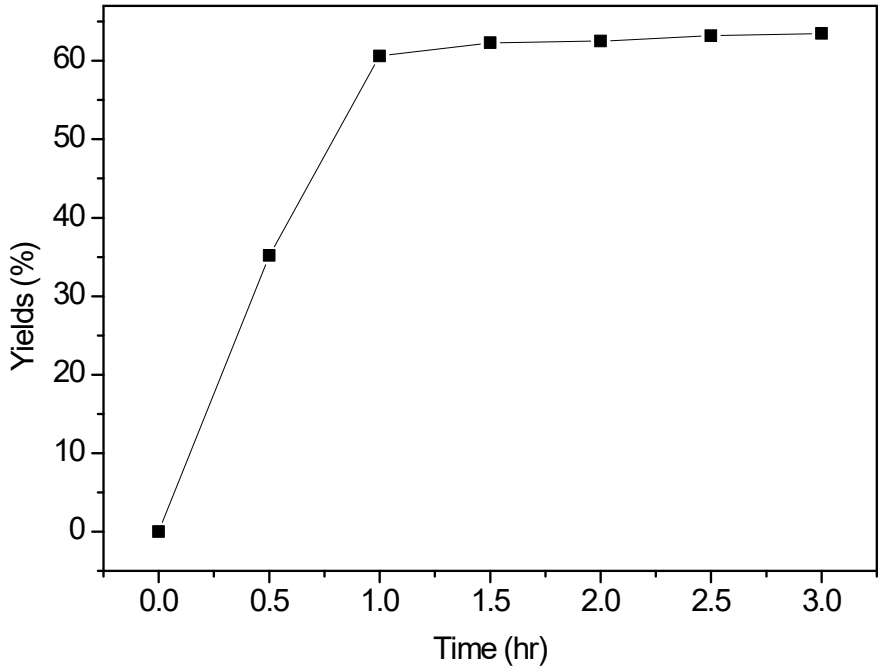

Figure S10. SEM image of [Cu_{20}] (left) and [Cu_{20}] after 5 cycles of catalysis (right).

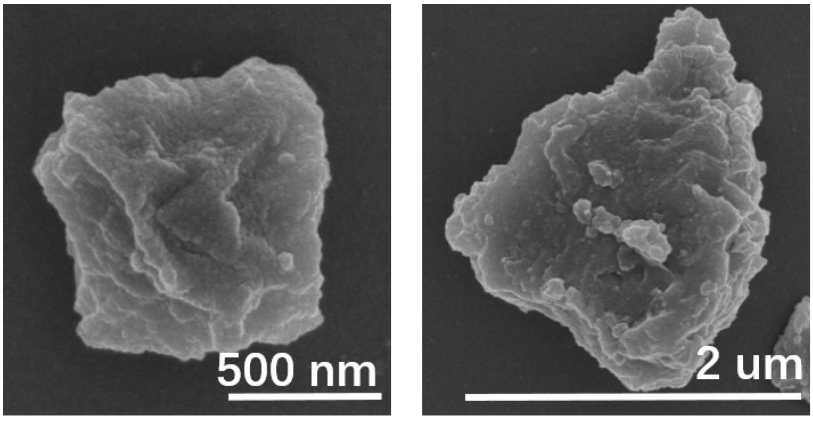

Figure S11. The FT-IR of the [Cu_{20}] catalysts before (black) and after (red) the catalytic reaction.

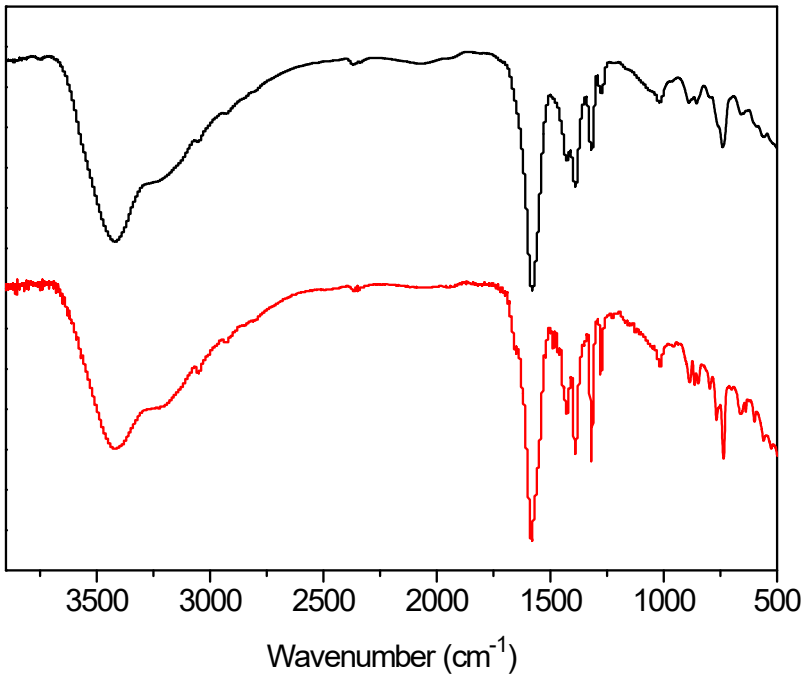

Table S3. Comparison with different catalysts in the cyclic addition of CO_2 and epichlorohydrin.

Entry	Catalyst	P (MPa)	T (℃)	T (hr)	TON	TOF	Ref.
1	PIL-R@MIL-101	1	80	2.5	292	116.7	[S1]
2	Co-salen-POP	1	100	0.5	1815	3630	[S2]
3	Zn(3,3'-L)	0.5	120	24	96	4	[S3]
4	PNU-25-NH_2	0.1	65	18	1500	83	[S4]
5	rho-ZMOF	1	40	3	1008	336	[S5]
6	MOF-53	1.6	100	2	975	488	[S6]
7	IL@MIL-101-SO_3H	0.1	90	48	2512	52	[S7]
8	Cu-BTC/UiO-66	1.2	60	8	15625	1953	[S8]
9	$Zr_6O_4(OH)_4(TzTz)_6$	0.1	120	24	295.2	12.3	[S9]
10	PNU-21/22	0.4	80	8	4167	521	[S10]
12	$[Cu_{20}]$	1.0	80	3	58823	19607	This work

Table S4. Control experiments of coupling of epichlorohydrin with CO_2.[a]

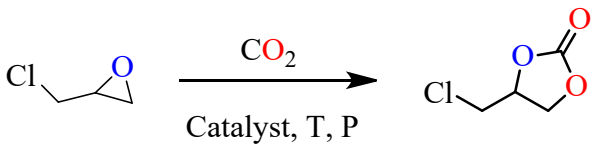

Entry	Catalyst	Co-catalyst	Yield(%)[b]	TON[c]	TOF[d]
1	none	none	*n.d.*	*n.d.*	*n.d.*
2	$[Cu_{20}]$	none	1	588	196
3	none	TBABr	*n.d.*	*n.d.*	*n.d.*
4	anthracene-9-carboxylic acid	TBABr	5	245	82
5	$CuBr_2$	none	6	176	59
6	$CuBr_2$	TBABr	42	1235	412
7	$[Cu_{20}]$	TBABr	>99	58823	19607
8	$[Cu_2]$	TBABr	16.7	9824	3275

[a] Reaction conditions: epichlorohydrin (10 mmol), catalyst (0.17 μmol based on $[Cu_{20}]$ and $[Cu_2]$, 2.04 μmol based on anthracene-9-carboxylic acid, and 3.4 μmol based on $CuBr_2$) and TBABr (0.3 mmol) under carbon dioxide (1 MPa), 353 K and 3 h. [b] Yield of isolated product was determined from by ^1H NMR spectroscopy. [c] Moles of cyclic carbonate per mole of catalyst. [d] Moles of cyclic carbonate per mole of catalyst per hour.

Reference

S1. Y. Jiang, D. Li, Y. Zhao and J. Sun, *J. Colloid Interf. Sci.*, 2022, **618**, 22-33.

S2. G. Yuan, Y. Lei, X. Meng, B. Ge, Y. Ye, X. Song and Z. Liang, *Inorg. Chem. Front.*, 2022, **9**, 1208-1216.

S3. G. Mercuri, M. Moroni, K. V. Domasevitch, C. Di Nicola, P. Campitelli, C. Pettinari, G. Giambastiani, S. Galli and A. Rossin, *Chem-Eur. J.*, 2021, **27**, 4746-4754.

S4. J. F. Kurisingal, Y. Rachuri, Y. Gu, R. K. Chitumalla, S. Vuppala, J. Jang, K. K. Bisht, E. Suresh and D.-W. Park, *ACS Sustain. Chem. Eng.*, 2020, **8**, 10822-10832.

S5. S. Zhang, M.-S. Jang, J. Lee, P. Puthiaraj and W.-S. Ahn, *ACS Sustain. Chem. Eng.*, 2020, **8**, 7078-7086.

S6. S. Demir, S. Usta, H. Tamar and M. Ulusoy, *Micropor. Mesopor. Mat.*, 2017, **244**, 251-257.

S7. Y. Sun, H. Huang, H. Vardhan, B. Aquila, C. Zhong, J. A. Perman, A. M. Al-Enizi, A. Nafady and S. Ma, *ACS Appl. Mater. Inter.*, 2018, **10**, 27124-27130.

S8. J. F. Kurisingal, Y. Rachuri, Y. Gu, G.-H. Kim and D.-W. Park, *Appl. Catal. A-Gen.*, 2019, **571**, 1-11.

S9. P. Mueller, B. Bucior, G. Tuci, L. Luconi, J. Getzschmann, S. Kaskel, R. Q. Snurr, G. Giambastiani and A. Rossin, *Mol. Syst. Des. Eng.*, 2019, **4**, 1000-1013.

S10. Y. Rachuri, J. F. Kurisingal, R. K. Chitumalla, S. Vuppala, Y. Gu, J. Jang, Y. Choe, E. Suresh and D.-W. Park, *Inorg. Chem.*, 2019, **58**, 11389-11403.